processes

MDPI

*Article*

# A New Model of Temperature Field Accounting for Acid–Rock Reaction in Acid Fracturing in Shunbei Oilfield

**Jianye Mou [2,*], Jiayuan He [1], Haiqian Zheng [2], Rusheng Zhang [1], Lufeng Zhang [1,*] and Budong Gao [2]**

[1] Key Laboratory of Marine Oil & Gas Reservoirs Production, Sinopec, Petroleum Exploration and Production Research Institute, Beijing 100083, China
[2] State Key Laboratory of Petroleum Resources and Engineering, China University of Petroleum, Beijing 102249, China
* Correspondence: moujianye@cup.edu.cn (J.M.); zlfcupb@163.com (L.Z.)

**Abstract:** The Shunbei oil formation is a deep, high-temperature carbonate reservoir. Acid fracturing is an effective technology to stimulate this formation. For acid fracturing, the temperature field is fundamental information for the acid system selection, acid–rock reaction, live acid penetration distance prediction, acid fracturing design, etc. Therefore, in this paper, we conduct a numerical study on the temperature field in acid fracturing to account for the acid–rock reaction in the Shunbei formation. Firstly, a new mathematical model of the fracture temperature field during acid fracturing is established based on the laws of mass and energy conservation and acid–rock reaction kinetics. The fracture model is based on a PKN model, which accounts for a few factors, such as the acid–rock reaction heat, acid–rock reaction rate dependence on the temperature, and the fracture width change with acid erosion. Then, the numerical mode is developed. Next, an extensive numerical study and a parameter analysis are conducted based on the model with the field data from the Shunbei formation. The study shows that the acid–rock reaction in acid fracturing has obvious effects on the temperature field, resulting in a 10~20 °C increase in the Shunbei formation. The acid–rock reaction dependence on temperature is a factor to be accounted for. The rock dissolution increases first and then decreases from the inlet to the tip of the fracture, unlike the monotonous decrease without temperature dependence. The temperature gradient is high near the inlet and then decreases gradually. Beyond half of the fracture, the temperature is close to the formation temperature. The temperature drops fast in the initial injection stage and tends to stabilize at about 50 min.

**Keywords:** temperature field; acid fracturing; acid–rock reaction; numerical simulation; Shunbei oilfield



**Citation:** Mou, J.; He, J.; Zheng, H.; Zhang, R.; Zhang, L.; Gao, B. A New Model of Temperature Field Accounting for Acid–Rock Reaction in Acid Fracturing in Shunbei Oilfield. *Processes* **2023**, *11*, 294. https://doi.org/10.3390/pr11010294

Academic Editor: Yidong Cai

Received: 30 December 2022
Revised: 9 January 2023
Accepted: 12 January 2023
Published: 16 January 2023



## 1. Introduction

Acid fracturing is primarily used in the stimulation of carbonate formations. The key to evaluating the effectiveness of acid fracturing is the effective acid fracture length and acid fracture conductivity. The effective acid fracture length depends on the live acid penetration distance. Among the parameters affecting the live acid penetration distance, the temperature is an important factor affecting the acid–rock reaction, rock dissolution, and acid viscosity and determining the effective acid action distance [1,2]. The Shunbei carbonate reservoir is characterized by a deep burial, high reservoir temperature, and high fracture pressure, compared with acid fracturing in other oilfields, and the high reservoir temperature and faster acid–rock reaction rate in the Shunbei oilfield result in a short effective acid penetration distance. Therefore, studying the temperature distribution within the fracture is essential to guide the design of the acid fracturing in deep formations under high-temperature and high-pressure conditions, which has far-reaching significance in selecting the optimal acid system and the treatment parameters [3–6].

The first model for calculating the fracture temperature field was proposed by Wheeler [7], who used an analytical solution to establish the relationship between the dimensionless

temperature and the factors such as the fracture width, injection rate, injection time, leak-off rate, and fluid and formation properties for a fixed fracture width and fluid loss. After summarizing the Wheeler model, Dysart and Whitsitt [8] first proposed a one-dimensional mathematical model (the D-W model) to calculate the fluid temperature distribution in a hydraulic fracture at a given distance from the wellbore with a fixed fracture width and a fixed fracture height. Nevertheless, they neglected the difference in the heat transfer between the fracturing fluid and the formation and the energy change caused by the heat convection of the fracturing fluid loss. Kamphuis et al. [9] researched the temperature field in a fracture and found that the heat transfer in the direction of the fracturing fluid flow is controlled by a convective heat transfer. In contrast, thermal diffusion controls the heat transfer in the direction perpendicular to the fracture walls. This led to the development of a mathematical model for the hydraulic fracture temperature based on the average fracture width (the K-D-R model), which is still widely used. Based on this, Ji [10] established a mathematical model for calculating the fracture temperature field of acid fracturing and considered the acid–rock reaction heat as a constant value by adding the acid–rock reaction heat to the energy equation, but he did not consider the fracture dimension change or the dependence of the acid–rock reaction on the temperature. Hu [11] developed a temperature model considering the acid–rock reaction during the acid fracturing of naturally fractured carbonate reservoirs, where wormholes form and thus affect the temperature distribution [12–15].

In this paper, based on the K-D-R model, a new temperature field model in acid fracturing is developed for the Shunbei carbonate formation. Compared to conventional models, this model considers the acid–rock reaction heat generated during acid fracturing and the dependence of the reaction rate on the temperature. Based on the model, extensive numerical simulations are conducted for a parameter analysis with the Shunbei formation properties. The finding in this paper can improve the acid system selection and parameter design of the acid fracturing treatment [16–19].

## 2. Mathematical Model

### 2.1. Physical Model

Considering the propagation of hydraulic fractures in the acid fracturing process, a physical model is established (Figure 1), which divides the fracture and peri-fracture temperature field during acid fracturing into three parts, namely the fluid temperature field in the fracture, temperature field in the leak-off zone, and temperature field in the formation. To facilitate the model solving, the following assumptions are adopted as other acid fracturing models [9,11] did: (1) The hydraulic fracture propagation conforms to the PKN model, i.e., the fracture height is constant and equal to the reservoir thickness. (2) The reservoir and injection fluid thermodynamic parameters are constant and do not vary with temperature, flow state, and other conditions. (3) The fluid flow within the fracture is stable and incompressible. (4) The reaction system's volume does not change during the acid–rock reaction, i.e., the volumes of the reactants and products are equal. (5) Energy changes due to fluid friction and volume changes are ignored [16]. (6) The formation is considered as 100% of calcite or dolomite.

The energy-coupling process between the fluid in the fracture and the bedrock of the formation is characterized by the following energy changes:

(1) Low-temperature acid fluid is continuously injected through perforations and leaks into the rock matrix. The energy of the formation around the fracture and the leak-off zone is constantly taken away, resulting in heat dissipation by leak-off.

(2) Heat conduction from the high-temperature formation to the low-temperature fluid in the fracture goes through the following processes: from the formation to the fracture leak-off zone and finally to the fluid in the fracture.

(3) Acid–rock reactions occur in the fracture wall when acid is injected, and a portion of the energy is released [20,21].

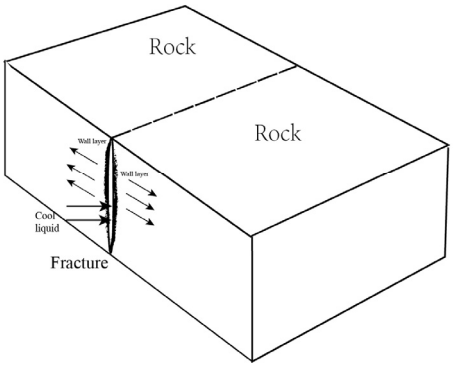


**Figure 1.** Physical model of the fracture temperature field for acid fracturing.

### *2.2. Governing Equations*

(1) The continuity equation

Based on the established physical model, the acid flow within the fracture satisfies the law of conservation of mass. An element within the fracture is assumed according to the flow process, as shown in Figure 2.

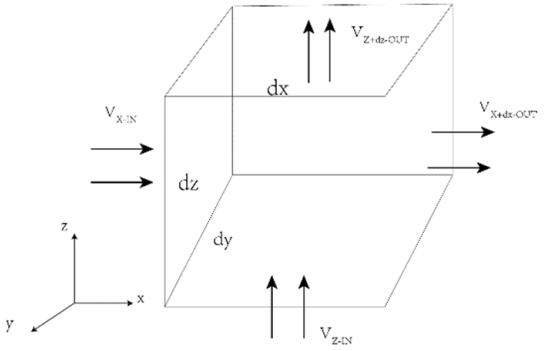


**Figure 2.** Schematic diagram of an element within the fracture.

A PKN model is implemented to calculate the fracture dimensions. Because the fracture width (y direction) is much smaller than the fracture length (x direction) and the fracture height (z direction), the fluid flow in the y direction can be neglected. The equation of fluid continuity within the fracture is obtained based on the law of conservation of mass:

$$\frac{\partial w V_x}{\partial x} + \frac{\partial w V_z}{\partial z} + 2V_{leak-off} = -\frac{\partial w}{\partial t} \quad (1)$$

where $w$ is the fracture width (m), $V_{z,x}$ is the velocity along the direction of the fracture length and height (m/s), $V_{leak-off}$ is the acid leak-off rate (m/s), and $t$ is the treatment time (s).

(2) Acid balance equation

The flow of the injected acid through the fracture is divided into two main parts: diffusion and leak-off. The diffusion part of the acid is the main source of acid to dissolve the rock wall, which contributes to the acid fracture wall dissolution and the fracture width widening. The liquid leak-off part of the acid flows into the formation, forming a leak-off zone, which is usually considered not to participate in the acid–rock reaction at the fracture wall, but the heat of the acid–rock reaction released from the leak-off zone is one of the energy sources in the fracture [22,23].

The reaction of carbonate rock with HCl is controlled by the mass transfer rate. The acid concentration at the fracture wall is much lower than that at the center of the fracture as the acid flows within the fracture. Therefore, the concentration gradient in the fracture width direction can be simplified to the extent that the acid concentration at the fracture wall can be approximated as zero. Therefore, the concentration gradient is expressed in terms of the effective mass transfer coefficient of hydrogen ions and the average acid concentration. That is,

$$-D\frac{\partial C}{\partial y}\,|_{y=\frac{w}{2}} = k_g(C - C_0) = k_g C \tag{2}$$

$C$ and $C_0$ denote the average acid concentration from the center of the fracture to the fracture wall and the acid concentration at the fracture wall, respectively. $k_g$ is the mass transfer coefficient (m/s).

According to the law of conservation of mass, the equation for the distribution of acid concentration in the fracture is as follows:

$$-\frac{\partial(Cv_x w)}{\partial x} - \frac{\partial(Cv_z w)}{\partial z} - 2(V_{leak-off} + k_g)C = \frac{\partial(Cw)}{\partial t} \tag{3}$$

(3) Fracture width variation

The acid reacting with the carbonate is believed to be mainly transported to the fracture wall by diffusion. In contrast, only a tiny amount of the leak-off acid is involved in the acid–rock reaction at the fracture wall. Most leak-off acid flows into the formation through wormholes, which is believed to make a small contribution to the fracture width increasement.

The mass conservation equation for the change in acid-etched fracture width per unit of time due to the dissolution of the fracture wall by the acid–rock reaction is as follows:

$$(2k_g C + 2\eta V_{leak-off} C)\frac{\beta}{\rho_r(1-\phi)} = \frac{\partial w}{\partial t} \tag{4}$$

where $k_g$ is the $H^+$ mass transfer coefficient (m/s), $\beta$ is the dissolving power of the acid, fractional, $\rho_r$ is the density of the rock (kg/m$^3$), and $\phi$ is the porosity of the formation. $\eta$ is the proportion of the acid that dissolves the rock on the surface of the fracture before the acid leaks into the formation, often taken as 30%.

(4) Energy conservation equation in the fracture

When the acid flows through the fracture, it is assumed that the temperature inside the element has reached thermal equilibrium and the temperature at the center of the fracture is $T$. The acid inside the fracture flows in the direction of the fracture length, on the one hand, and leaks off along the direction perpendicular to the fracture wall, on the other.

Considering the incompressible fluid, ignoring the effect of kinetic energy on the internal energy of the fluid, and assuming that heat conduction is thermally homogeneous, the energy conservation equation for the fluid in the fracture is as follows.

$$\begin{aligned}\rho_f c_f \frac{\partial w T_f}{\partial t} = -\rho_f c_f\left(\frac{\partial w T_f v_x}{\partial x} + \frac{\partial w T_f v_z}{\partial z}\right) + k_f\left(\frac{\partial^2 w T_f}{\partial x^2} + \frac{\partial^2 w T_f}{\partial z^2}\right)\\ +Q_r - Q_{leak-off}\end{aligned} \tag{5}$$

where $c_f$ is the specific heat capacity of the acid (J/(kg·°C)), $\rho_f$ is the density of the acid (kg/m$^3$), $k_f$ is the acid thermal conductivity (W/(m·°C)), $T_f$ is the acid temperature (°C), $w$ is the fracture width (m), and $T_d$ is the temperature of the leak-off zone (°C). $v$ is the velocity of the acid in the fracture (m/s).

$$Q_r = 2h_d\left(T_d - T_f\right) \tag{6}$$

$$Q_{leak-off} = 2c_f\rho_f V_{leak-off} T_f \tag{7}$$

where $V_{leak-off}$ is the acid leak-off rate (m/s) and $h_d$ is the convective heat transfer coefficient. The convective heat transfer coefficient satisfies the following equation under the condition that the heat transfer at the fracture surface conforms to Fourier's law.

$$h_d \approx \frac{k_f}{\delta_T} \tag{8}$$

The thickness of the temperature boundary layer decreases as the velocity increases and is more difficult to describe accurately, so the average thickness of the boundary layer is usually assumed. Meanwhile, Plante [10] suggests that if the acid velocity along the object's surface is sufficiently high, the temperature boundary layers are very thin, and the boundary layer approximation can be used. The convective heat transfer coefficient for a fully developed temperature field is calculated as follows.

$$h_d = \frac{k_f Nu}{w} \tag{9}$$

where $Nu$ is the Nussle number, and it usually takes 4~5.

(5) Energy conservation equation in leak-off zone

Compared with the fracture length, the leak-off zone is small, and the temperature distribution of the leak-off zone in the direction perpendicular to the fracture wall can be ignored. It is assumed that the temperature gradient of the leak-off zone is considered in the direction of the fracture length and fracture height. As a result, the energy conservation of an element in the leak-off zone can be described as follows: the sum of the energy flowing into the element and the energy introduced by the acid–rock reaction minus the energy flowing out of the element is equal to the total energy change in the element in the leak-off zone. The energy equation for the leak-off zone is written as follows:

$$\begin{aligned} &\xi\left[c_f\rho_f\phi + c_r\rho_r(1-\phi)\right]\tfrac{\partial T_d}{\partial t} \\ &= c_f\rho_f V_{leak-off}\left(T_f - T_d\right) + k_{ef}(T_{res} - T_d)\tfrac{1}{\sqrt{\pi D\tau}}\tfrac{e^{-\frac{F^2}{D}}}{1+erf\left(\frac{F}{\sqrt{D}}\right)} \\ &+ \tfrac{k_f Nu}{w}\left(T_f - T_d\right) + (2k_g\overline{C} + V_{leak-off}\phi k_g\overline{C}\Delta t) \times \Delta H_{HCl} \end{aligned} \tag{10}$$

$$F = \frac{c_f\rho_f C_t}{c_f\rho_f\phi + c_r\rho_r(1-\phi)} \tag{11}$$

$$D = \frac{K_{ef}}{c_f\rho_f\phi + c_r\rho_r(1-\phi)} \tag{12}$$

$$k_{ef} = k_r(1-\varphi) + k_f\varphi \tag{13}$$

where $T_d$ is the temperature of the leak-off zone (°C); $c_f$ is the specific heat capacity of the acid (J/(kg·°C)); $c_r$ is the specific heat capacity of formation rock (J/(kg·°C)); $\rho_r$ is the density of formation rock (kg/m$^3$); $\rho_f$ is the density of the acid (kg/m$^3$); $\phi$ is the porosity, fractional; $\xi$ is the leak-off zone thickness (m); $V_{leak-off}$ is the acid leak-off rate (m/s); $C_t$ is the integrated leak-off factor ($m/\sqrt{\text{min}}$); $\Delta t$ is the time step; and $T_f$ is the acid temperature (°C).

The energy equation for the leak-off zone consists of four components: convective heat exchange, heat transfer between the fluid in the fracture and the leak-off zone, heat transfer between the in situ rock and the leak-off zone, and heat generation by the acid–rock reaction [17]. The equation can be solved by coupling the energy changes in these four components to achieve an energy balance.

The following equation gives the enthalpy of the reaction between hydrochloric acid and limestone during acid fracturing, considering the temperature and pressure conditions [24].

$$\begin{aligned}\Delta H_m^{\Theta}(T,p) &= -13.692 + \tfrac{1}{1000}(-6.443\times10^{-3}T^2 + 16.075T - \tfrac{17.406\times10^5}{T}) \\ &\quad + \int_{1atm}^{p} V_{co_2}[V_{co_2} - T(\tfrac{\partial V_{co_2}}{\partial T})_p]_T dp\end{aligned} \tag{14}$$

The enthalpy of the reaction of dolomite with hydrochloric acid is calculated as follows:

$$\begin{aligned}\Delta H_m^{\Theta}(T,p) &= -43.272 + \tfrac{1}{1000}(-21.508\times10^{-3}T^2 + 49.552T - \tfrac{1.46\times10^5}{T}) \\ &\quad + \int_{1atm}^{p} V_{co_2}[V_{co_2} - T(\tfrac{\partial V_{co_2}}{\partial T})_p]_T dp\end{aligned} \tag{15}$$

where $\Delta H_m^{\Theta}(T,p)$ is the standard molar reaction enthalpy of limestone ($kJ/mol$) and $V_{co_2}$ is the molar volume of $CO_2$, determined by the relevant equation of state; $P$ and $T$ are pressure (atm) and temperature (°C) at which the acid–rock reaction takes place.

(6) Initial conditions and boundary conditions

Initial conditions for the model:

$$\begin{aligned}T_d(x,z,t)|_{t=0} &= T_{res} \\ T_f(x,z,t)\Big|_{t=0} &= T_{res}\end{aligned} \tag{16}$$

Boundary conditions for the model:

$$\begin{aligned}&T(x,z,t)|_{x=0} = T_{inject} \\ &T(x,z,t)|_{x=L} = T_{res} \\ &C(x,z,t)|_{x=0} = C_{inject} \\ &\tfrac{\partial p}{\partial x}\Big|_{x=0} = -\tfrac{12\mu q}{Sw^2} \\ &p_{x=L} = p_e\end{aligned} \tag{17}$$

where $T_{inject}$ is the temperature of injected acid (°C), $C_{inject}$ is the acid concentration (wt.%) and $q$ is the injection rate, $S$ is the cross-sectional area of inlet ($m^2$), $\mu$ is the acid viscosity (Pa·s), and $w$ is the fracture width of inlet (m).

## 3. Numerical Implementation Process

The numerical model of the temperature field is discretized according to the finite difference method, and a block-centered grid is used to mesh the fracture along the fracture length direction. The overall numerical implementation process of the temperature field model is summarized as follows.

(1) Input the formation parameters, treatment parameters, physical properties of the injected fluid, etc.

(2) The hydraulic fracture dimensions (fracture length and width) at the current time step are derived from the input parameters based on the PKN model, and then the fracture meshes into girds.

(3) Calculate the continuity equation based on the law of conservation of mass to obtain the pressure and velocity fields within the fracture.

(4) Based on the pressure and velocity fields, the acid concentration distribution in the fracture at the current time step is calculated, and the acid-etched fracture width is calculated based on the acid–rock reaction. The fracture dimension parameters are updated.

(5) Considering the heat generated by the acid–rock reaction and assuming that the distribution of the fluid temperature field in the fracture is $T_{f0}$, based on the updated fracture parameters and the initial conditions of the formation, calculate the temperature field in the leak-off zone under the current temperature–pressure conditions.

(6) Calculate the fluid temperature field in the fracture $T_f$ at the current temperature and pressure condition based on the temperature field in the leak-off zone derived in step (5). Compare the magnitude of $T_f$ with the assumed $T_{f0}$. If the calculated result $T_f$ does not meet the error requirement $\left|T_{f0} - T_f\right| \leq \varepsilon$, then set $T_{f0} = T_f$ and repeat steps (5) to (6) until the computed result meets the error requirement. The temperature field of the fluid and the leak-off zone in the current time step are obtained.

(7) Repeat steps (2) to (6) until the entire acid fracturing process is completed.

## 4. Results and Analysis

### 4.1. Data for Simulation

To analyze the factors affecting the fracture temperature field during acid fracturing, a simulation study was conducted using actual data from the Shunbei carbonate reservoir. Taking Shunbei well #T as an example, the well was designed to stimulate with acid fracturing in an open-hole section ranging from 6550.00 to 6781.63 m to create acid-etched fractures. The reservoir lithology is mainly micrite, in which the content of calcite is more than 95%, quartz about 4%, and clay about 1%. In addition, the pressure gradient in the area is 1.10, which is a normal pressure reservoir. The regional stratigraphic temperature gradient is 2.26 °C/100 m, with an expected reservoir temperature of 145.2 °C at a mid-depth of 6424.0 m.

The treatment parameters, rock mechanical properties, and thermodynamic properties are given in Table 1 below, and the injection parameters are given in Table 2 below.

**Table 1.** Treatment parameters and stratigraphic parameters for Shunbei well #T.

| Parameters (Units) | Value | Parameters (Units) | Value |
|---|---|---|---|
| Reservoir depth (m) | 6500 | Geothermal gradients (°C/m) | 0.0226 |
| Reservoir temperature (°C) | 145.2 | Porosity (%) | 0.2 |
| Fracture height (m) | 50 | Temperature of injected fluid (°C) | 25 |
| Injection rate ($m^3$/min) | 5~7 | Young's modulus of the rock (MPa) | 36,700 |
| Poisson ratio | 0.26 | Thermal conductivity of the rock (W/(m·K)) | 5.2 |
| Density of the rock (kg/$m^3$) | 2700 | Specific heat capacity of the reservoir crude oil (J/(kg·K)) | 1981 |
| Specific heat capacity of the reservoir rock (J/(kg·K)) | 999 | Thermal conductivity of crude oil (W/(m·K)) | 0.339 |
| Density of crude oil (kg/$m^3$) | 840 | - | - |

**Table 2.** Injection parameters for Shunbei well #T.

| Parameters (Units) | Value | Parameters (Units) | Value |
|---|---|---|---|
| Density (kg/$m^3$) | 1090–1110 | Specific heat capacity (J/(kg·K)) | 4180 |
| Coefficient of thermal conductivity (W/(m·K)) | 0.65 | Acid concentration (%) | 15 |
| Acid–rock reaction rate constant (mol/$cm^3$) | $0.9849 \times 10^{-6}$ | The heat generated by the acid–rock reaction (kJ/mol) | $\Delta H_m^{\Theta}(T, p)$ |
| Order of the reaction (dimensionless) | 0.88 | Mass transfer coefficient (m/s) | $1.4693 \times 10^{-5}$ |

### 4.2. Effect of Acid–Rock Reaction Heat on Temperature Distribution

To investigate the effect of the reaction heat on the temperature distribution in the fracture, two simulation cases are performed, one considering the reaction heat and the other not. Viscous acid with an injection rate of 6 $m^3$/min and a temperature of 25 °C is injected for 90 min. Figures 3 and 4 show the simulation results. The temperature inside the fracture gradually increases along the fracture and eventually approaches the formation temperature. Comparing the distribution of the fluid temperature and the leak-off zone temperature with and without considering the reaction heat, it can be found that the acid–rock reaction heat has a significant effect on the distribution of the temperature in the fracture. It results in a maximum temperature difference of 15 °C. The temperature difference is slight at the two ends of the fracture but significant in the middle. The potential

reason is that the temperature at the inlet of the fracture is low due to the continuous injection of the cool acid, which leads to a slow acid–rock reaction. At the fracture tip, the temperature is close to the formation temperature, and the concentration of the acid is low, sometimes becoming residual acid, which also has little effect on the reaction heat. The acid concentration in the middle of the fracture is high, and the fracture temperature is relatively high, so the acid–rock reaction rate is fast, and the effect of the reaction heat on the temperature distribution is significant (Figure 5). Therefore, the acid–rock reaction heat cannot be ignored in the fracture temperature calculation.

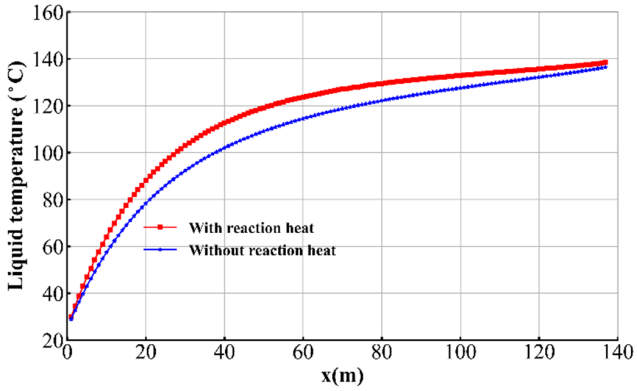


**Figure 3.** Temperature distribution of the fluid in the fracture (blue line: without reaction heat; red line: considering reaction heat).

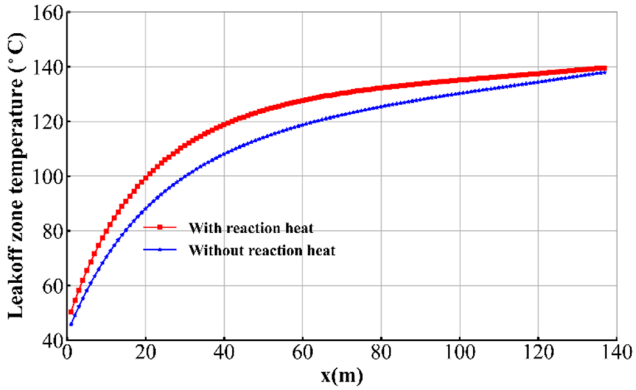


**Figure 4.** Temperature distribution of the leak-off zone (blue line: without reaction heat; red line: considering reaction heat).

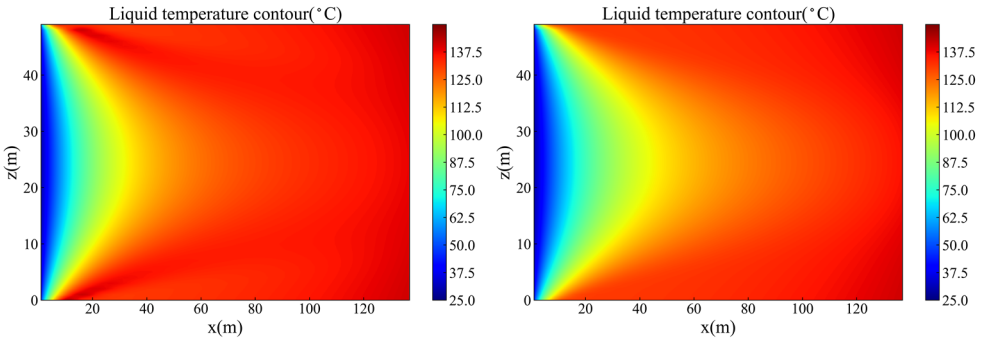


(**a**) (**b**)

**Figure 5.** Thermal map of fluid temperature distribution in the fracture leak-off zone with and without considering acid–rock reaction heat. (**a**) considering reaction heat, (**b**) without considering reaction heat.

### *4.3. Effect of Acid Properties on Temperature Field*

The reaction rates between different acids and carbonate rocks vary, among which the reaction rate between limestone and the acid is mainly determined by the mass transfer rate. The effect of the temperature variation on the mass transfer coefficients of different acid species is discussed in this section. Table 3 and Figure 6 show the variation in the mass transfer coefficients of three commonly used acids in the oilfield at different temperatures. In our paper, plain acid refers to HCl with a mass concentration of 15%, gelled acid is obtained from a plain acid mixing with additives such as gelling agents, and crosslinked acid refers to the acid obtained by adding an organic polymer crosslinking agent to plain acid (HCl of 15%wt). Because the viscosity of different acid species differs, the fracture dimensions formed vary. To eliminate the influence of the fracture dimensions, the fracture dimension created by three acid species was set the same in the model. The mass transfer coefficient of plain acid is significantly affected by the temperature, while the gelled acid and crosslinked acid were less affected. Figure 7 shows the distribution of the acid-etched fracture width of the injecting plain acid, gelled acid, and crosslinked acid, considering the variation in the mass transfer coefficient with the temperature. Figure 8 demonstrates a two-dimensional fracture width distribution of the injecting plain acid and crosslinked acid. Compared with the acid-etched fracture width under the constant mass transfer coefficient shown in Figure 9, it is concluded that when considering the variation in the mass transfer coefficient with the temperature, the acid–rock reaction rate decreases at the inlet of the fracture due to the cooling effect of the continuous injection, and the maximum acid-etched fracture width offsets the fracture inlet. Meanwhile, when considering the cooling effect, the maximum etched fracture width is less, and the live acid penetration distance is longer than those without considering the cooling effect.

**Table 3.** Variation in mass transfer coefficients with temperature for three commonly used acids in the field.

| Temperature (°C) | Acid Concentration (mol/L) | Mass Transfer Coefficient ($10^{-5}$ m/s) | | |
|---|---|---|---|---|
| | | Plain Acid | Gelled Acid | Plain Acid |
| 20 | 4.5 (15%wt) | 1.348 | 0.451 | 0.058 |
| 60 | 4.5 (15%wt) | 3.254 | 1.086 | 0.321 |
| 100 | 4.5 (15%wt) | 5.89 | 1.685 | 0.532 |
| 140 | 4.5 (15%wt) | 7.956 | 2.351 | 0.776 |
| 160 | 4.5 (15%wt) | 9.034 | 2.649 | 0.918 |

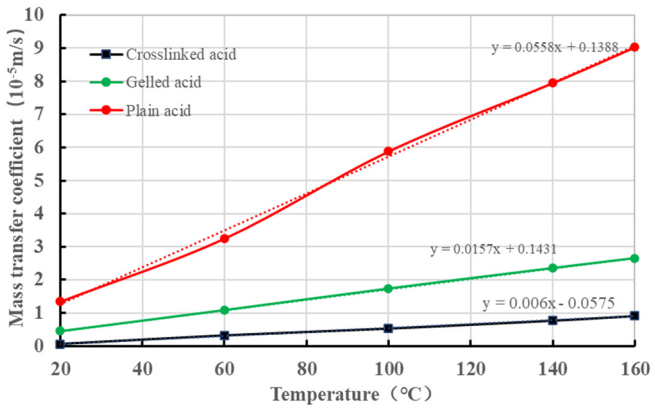


**Figure 6.** Modeling the temperature dependence of mass transfer coefficients for three acid species.

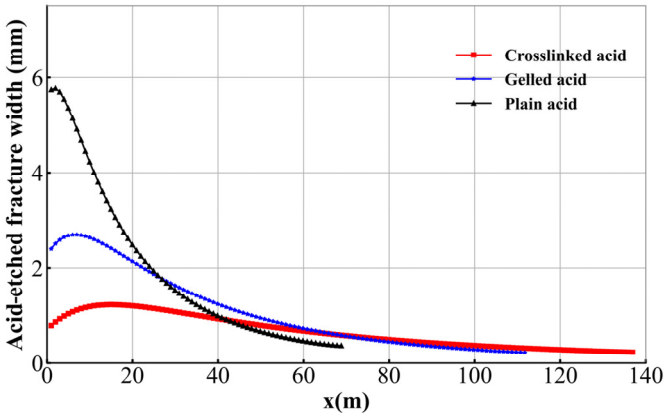


**Figure 7.** Acid-etched fracture width distribution of different acid solutions when considering the variation in mass transfer coefficient with temperature.

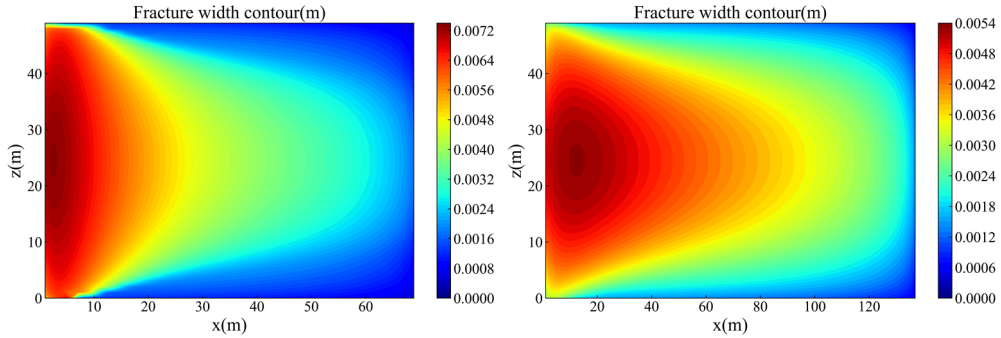


(**a**) (**b**)

**Figure 8.** Two-dimensional acid-etched fracture width distribution by injection of plain acid and crosslinked acid (considering the variation in mass transfer coefficient with temperature). (**a**) plain acid, (**b**) crosslinked acid.

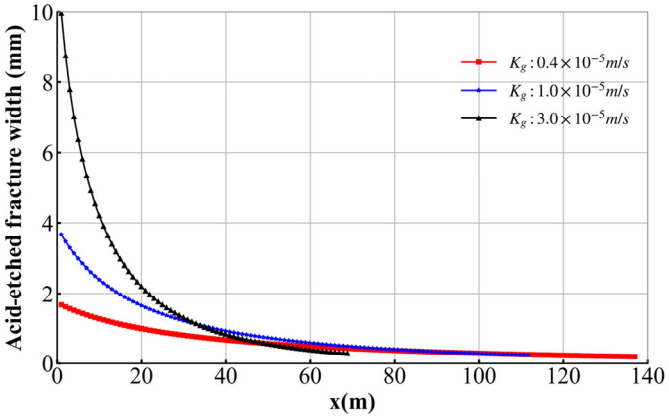


**Figure 9.** Acid-etched fracture width distribution under constant mass transfer coefficient (without considering the variation in mass transfer coefficient with temperature).

### *4.4. Temperature Field in Time Sequence*

The cooling effect comes into play mainly in the first third of the fracture, where the temperature decreases sharply with a large reduction, whereas the temperature of the other part of the fracture is close to the initial formation temperature. Comparing the temperature changes after different injection times (Figures 10 and 11), it can be seen that as the injection time increases, the fracture temperature at a given location decreases, but the cooling rate

gradually becomes slower, and the cooling area is concentrated in the middle front of the fracture. This is because as the cool fluid is injected, the fracture temperature continues to decrease. With the temperature difference decreasing, it becomes more difficult to lower the fracture temperature, and the temperature in the fracture gradually reaches a dynamic equilibrium state. Figure 12 shows the range, degree, and distribution pattern of the overall cooling effect after a period of injection.

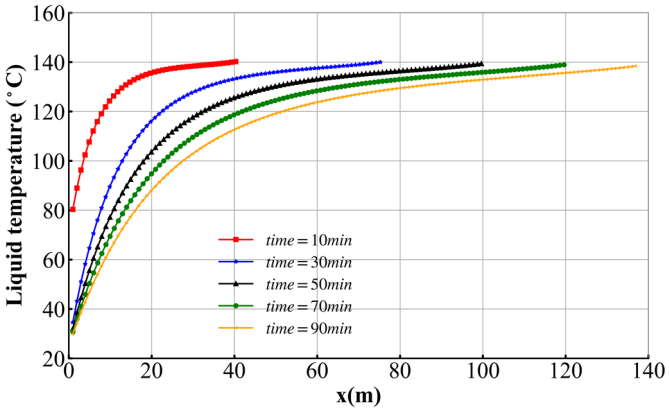


**Figure 10.** Fluid temperature distribution in the fracture at different injection times.

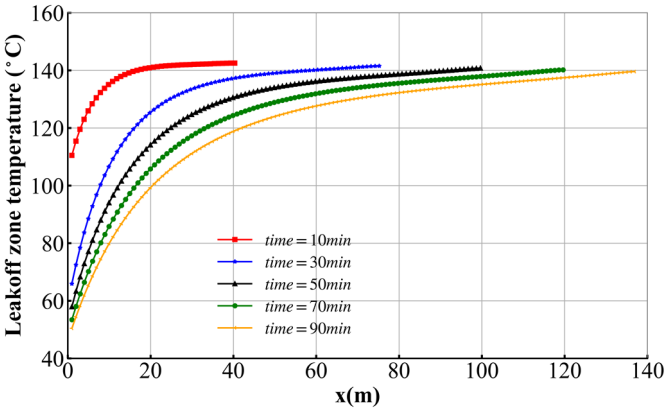


**Figure 11.** Temperature distribution in the leak-off zone at different times.

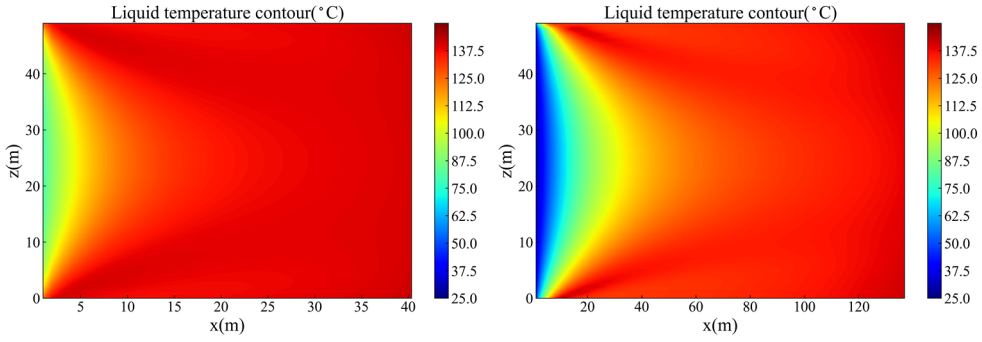


(**a**) (**b**)

**Figure 12.** Thermal maps of the fluid in the fracture at 10 and 90 min. (**a**) 10 min, (**b**) 90 min.

## 5. Conclusions

This paper develops a new temperature field model of acid fracturing in the Shunbei carbonate formation. The model accounts for the acid–rock reaction heat and the dependence of the acid–rock reaction rate on the temperature. Based on the extensive numerical simulations, the following conclusions can be reached:

(1) The acid–rock reaction in acid fracturing obviously affects the temperature field, resulting in about a 10~20 °C increase in the Shunbei formation.

(2) The acid–rock reaction rate dependence on the temperature is a vital factor that should be accounted for. The rock dissolution increases first and then decreases from the inlet to the tip of the fracture, unlike the monotonous decrease without the temperature dependence.

(3) The temperature gradient is high near the inlet and then decreases gradually. Beyond half of the fracture, the temperature is close to the formation temperature.

(4) The temperature decreases fast in the initial injection stage and tends to stabilize at about 50min.

**Author Contributions:** Conceptualization, J.M.; Formal analysis, H.Z.; Funding acquisition, J.H.; Methodology, J.M. and H.Z.; Project administration, R.Z.; Resources, J.H. and L.Z.; Supervision, J.M. and L.Z.; Writing—original draft, H.Z.; Writing—review and editing, B.G. All authors have read and agreed to the published version of the manuscript.

**Funding:** This research was funded by Key Laboratory of Marine Oil & Gas Reservoirs Production, Sinopec, grant number: 33550000-22-ZC0613-0311 and by Science and Technology Department, Sinopec, grant number: P21063-3.

**Data Availability Statement:** Not applicable.

**Acknowledgments:** This work is supported by the Open Fund Project for Numerical Simulation of Multiple-Cluster Fracture Propagation in Horizontal Wells during Acid Fracturing of a Carbonate Formation (No. 33550000-22-ZC0613-0311) provided by Key Laboratory of Marine Oil & Gas Reservoirs Production, Sinopec and by the Project Research on Key Engineering Technologies of Unused Reserves Development in Tahe Oilfield (P21063-3) provided by Science and Technology Department, Sinopec.

**Conflicts of Interest:** The authors declare no conflict of interest.

## Nomenclature

| | |
|---|---|
| $C_t$ | the integrated leak-off factor ($m/\sqrt{\text{min}}$) |
| $C_{inject}$ | the acid concentration (wt.%) |
| $C$ | the average acid concentration from the center of the fracture to the fracture wall (wt.%) |
| $C_0$ | the acid concentration at the fracture wall (wt.%) |
| $\Delta H_m^{\Theta}(T,p)$ | the standard molar reaction enthalpy of limestone (kJ/mol) |
| $S$ | the cross-sectional area of inlet ($m^2$) |
| $T_f$ | the acid temperature (°C) |
| $T_d$ | the temperature of the leak-off zone (°C) |
| $T_{inject}$ | the temperature of injected acid (°C) |
| $V_{co_2}$ | the molar volume of $CO_2$ |
| $V_{z,x}$ | the velocity along the direction of the fracture length and height (m/s) |
| $V_{leak-off}$ | the acid leak-off rate (m/s) |
| $Nu$ | the Nussle number, and it usually takes 4~5 |
| $c_f$ | the specific heat capacity of the acid (J/(kg·°C)) |
| $c_r$ | the specific heat capacity of formation rock (J/(kg·°C)) |
| $h_d$ | the convective heat transfer coefficient |
| $k_g$ | the mass transfer coefficient (m/s) |
| $k_f$ | the acid thermal conductivity (W/(m·°C)) |
| $q$ | the injection rate ($m^3$/min) |
| $t$ | the treatment time (s) |
| $\Delta t$ | the time step |
| $w$ | the fracture width (m) |
| $\beta$ | the dissolving power of the acid, fractional |
| $\rho_f$ | the density of the acid (kg/$m^3$) |
| $\rho_r$ | the density of formation rock (kg/$m^3$) |

| | |
|---|---|
| $\phi$ | the porosity of the formation |
| $\eta$ | the proportion of the acid that dissolves the rock on the surface of the fracture before the acid leaks into the formation, often taken as 30% |
| $\xi$ | the leak-off zone thickness (m) |
| $\mu$ | the acid viscosity (Pa·s) |

## References


1. Aljawad, M.S.; Zhu, D.; Hill, A.D. Temperature and geometry effects on the fracture surfaces dissolution patterns in acid fracturing. In Proceedings of the SPE Europec featured at 80th EAGE Conference and Exhibition, Copenhagen, Denmark, 11–14 June 2018. SPE-190819-MS.
2. Jawad, M.S.H.A. Development of a Fully Integrated Acid Fracture Model. Ph.D. Thesis, The University of Texas at Austin, College Station, TX, USA, 2018.
3. Guo, J.C.; Ren, J.C.; Wang, S.B. Numerical simulation and application of multi-field coupling of acid fracturing in fractured tight carbonate reservoirs. *Acta Pet. Sin.* **2020**, *41*, 1219.
4. Li, T.; Wang, S.B. Research on Acid Rock Reaction Model in High Temperature Carbonate Fracture. In Proceedings of the IPPTC Organizing Committee, Shanghai, China, 26 August 2020; p. 10.
5. Luo, P.D.; Li, H.Y.; Zhai, L.J.; Li, C.Y.; Lv, X.R.; Mou, J.Y. Supercritical $CO_2$ fracturing wellbore and fracture temperature field in Tahe Oilfield. *Fault-Block Oil Gas Field* **2019**, *26*, 225–230.
6. Khormali, A.; Sharifov, A.R.; Torba, D.I. The control of asphaltene precipitation in oil wells. *Pet. Sci. Technol.* **2018**, *36*, 443–449. [CrossRef]
7. Wheeler, J.A. Analytical calculations for heat transfer from fractures. In Proceedings of the SPE Improved Oil Recovery Symposium, Tulsa, OK, USA, 13–15 April 1969. SPE-2494-MS.
8. Dysart, G.R.; Whitsitt, N.F. Fluid temperature in fractures. In Proceedings of the fall meeting of the society of petroleum engineers of AIME, New Orleans, LA, USA, 1–4 October 1967. SPE-1902-MS.
9. Kamphuis, H.; Davies, D.R.; Roodhart, L.P. A new simulator for the calculation of the in-situ temperature profile during well stimulation fracturing treatments. *J. Can. Pet. Technol.* **1993**, *32*, 38–47. [CrossRef]
10. Ji, W. Research of Acid Fracturing Temperature Field Model with Considering Acid-Rock Reaction Heat. Ph.D. Thesis, Chengdu University of Technology, Chengdu, China, 2010.
11. Hu, J.Y. Modeling the Acidification Temperature Field of Horizontal Wells in Fractured Carbonate Reservoirs. Ph.D. Thesis, Southwest Petroleum University, Chengdu, China, 2016.
12. Biot, M.A.; Masse, L.; Medlin, W.L. Temperature analysis in hydraulic fracturing. *J. Pet. Technol.* **1987**, *39*, 1389–1397. [CrossRef]
13. Liu, W.; Zeng, Q.; Yao, J. Numerical simulation of elasto-plastic hydraulic fracture propagation in deep reservoir coupled with temperature field. *J. Petrol. Sci. Eng.* **2018**, *171*, 115–126. [CrossRef]
14. Ben, N.K.; Stephenson, P. Models of heat transfer in hydraulic fracturing. In Proceedings of the SPE/DOE Low Permeability Gas Reservoirs Symposium, Denver, CO, USA, 19 May 1985. SPE-13865-MS.
15. Wang, T.; Yang, Y.; Peng, Y.; Zhao, J.; Qi, T.; Zeng, J. Simulation and evaluation for acid fracturing of carbonate reservoirs based on embedded discrete fracture model. *Nat. Gas Ind. B* **2021**, *8*, 637–649. [CrossRef]
16. Guo, J.; Liu, H.; Zhu, Y.; Liu, Y. Effects of acid–rock reaction heat on fluid temperature profile in fracture during acid fracturing in carbonate reservoirs. *J. Petrol. Sci. Eng.* **2014**, *122*, 31–37. [CrossRef]
17. Liu, H.F.; Baletabieke, B.; Wang, G. Influences of real-time acid-rock reaction heat on etched fracture dimensions during acid fracturing of carbonate reservoirs and field applications. *Heliyon* **2022**, *8*, e11659. [CrossRef] [PubMed]
18. Dong, C. Acidizing of Naturally Fractured Carbonate Formations. Ph.D. Thesis, The University of Texas at Austin, Austin, TX, USA, 2001.
19. Zhai, W.B. Mechanism of Fractures Propagation of Multi-Stage Fracturing in Heterogeneous Shale Reservoir. Ph.D. Thesis, China University of Petroleum (Beijing), Beijing, China, 2020.
20. Xian, C. Study on the Temperature of Self-Generated Solid Phase Chemical Fracturing. Ph.D. Thesis, Southwest Petroleum University, Chengdu, China, 2018.
21. Wang, L.; Shen, X.Y.; Wang, R. Effects of acid-rock reaction heat on fracture temperature field and effective distance of live acid. *J. Chongqing Univ. Sci. Technol.* **2014**, *16*, 21–24.
22. John, D. Measuring diffusion coefficients in acid fracturing fluids and their application to gelled and emulsified acids. In Proceedings of the SPE Annual Technical Conference and Exhibition, New Orleans, LA, USA, 25–28 September 1994; SPE-28552-MS.
23. Xu, H.R.; Cheng, J.R.; Zhao, Z.H. Numerical study and application of acid-fracturing in the carbonate geothermal reservoirs from North China. *Acta Geol. Sin.* **2020**, *94*, 2157–2165.
24. Liu, H.F.; He, C.M.; Zhu, Y.Q. Method to calculate acid-rock reaction heat during acid fracturing of carbonate reservoir. *Nat. Gas Explor. Dev.* **2011**, *34*, 84–87+91+102–103.